Structural and Kinetic Analysis of Catalysis by a Thiamin Diphosphate-Dependent Enzyme, Benzoylformate Decarboxylase†

Elena S. Polovnikova,‡,§ Michael J. McLeish,|| Eduard A. Sergienko,⊥ John T. Burgner,‡ Natalie L. Anderson,‡ Asim K. Bera,‡ Frank Jordan,⊥ George L. Kenyon,|| and Miriam S. Hasson*,‡

Department of Biological Sciences, Purdue University, West Lafayette, Indiana 47907-1392, The College of Pharmacy, University of Michigan, Ann Arbor, Michigan 48109-1065, and Department of Chemistry and Program in Cellular and Molecular Biodynamics, Rutgers, the State University of New Jersey, Newark, New Jersey 07102

Received July 21, 2002; Revised Manuscript Received December 19, 2002

ABSTRACT: Benzoylformate decarboxylase is a member of the family of enzymes that are dependent on the cofactor thiamin diphosphate. A structure of this enzyme binding (*R*)-mandelate, a competitive inhibitor, suggests that at least two hydrogen bonds are formed between the substrate, benzoylformate, and active site side chains. The first is between the carboxylate group of benzoylformate and the hydroxyl group of S26, and the second is between carbonyl group of the substrate and an imidazole nitrogen of H70. Steady-state kinetic studies indicate that the catalytic parameters are strongly affected in three active site mutants, S26A, H70A, and H281A. The K_m of S26A was increased most dramatically, 25-fold more than that of the wild-type enzyme, while the K_i of (*R*)-mandelate was increased 100-fold, suggesting that the serine hydroxyl is important for substrate binding. The k_{cat} of H70A is reduced more than 3 orders of magnitude, strongly implicating this residue in catalysis, and H281 showed significant, but smaller magnitude, effects on both K_m and k_{cat}. Stopped-flow experiments using an alternative substrate, *p*-nitrobenzoylformate, lead to kinetic resolution of the fate of key thiamin diphosphate-bound intermediates. Together, the experimental results suggest the following roles for residues in the active site. The residue H70 is important for the protonation of the 2-α-mandelyl-ThDP intermediate, thereby assisting in decarboxylation, and for the deprotonation of the 2-α-hydroxybenzyl-ThDP intermediate, aiding product release. H281 is involved in protonation of the enamine. Surprisingly, S26 appears to be involved not only in substrate binding but also in other steps of the reaction.

Benzoylformate decarboxylase (BFD,[1] EC 4.1.1.7), which catalyzes the conversion of benzoylformate (Chart 1) to benzaldehyde and carbon dioxide, is a member of the family of enzymes that are dependent on thiamine diphosphate (ThDP). BFD is found in several closely related microorganisms as part of a pathway for degradation of mandelate (*1*−*7*). The mandelate pathway allows bacteria to use (*R*)-mandelate as a sole carbon source by converting it to benzoic acid, which is then metabolized by the β-ketoadipate pathway and the citric acid cycle (*2*−*4*). The enzymes of this recently evolved pathway have attracted interest as models for the studies of enzyme functional evolution (*8*). BFD from *Pseudomonas putida* is a tetramer of 56.2 kDa subunits (*9*, *10*). Its protein sequence is 25% identical to the sequence of yeast pyruvate oxidase (POX) and 21% identical to the sequence of yeast pyruvate decarboxylase (PDC) (*9*). BFD is an especially convenient model enzyme for the study of ThDP-dependent enzymatic catalysis. The protein is stable and can be easily expressed and purified (*10*), and its high-resolution crystal structure is available (*9*). In addition, the

Chart 1: Structures of Benzoylformate, (*R*)-Mandelate, and *p*-Nitrobenzoylformate (NBFA)

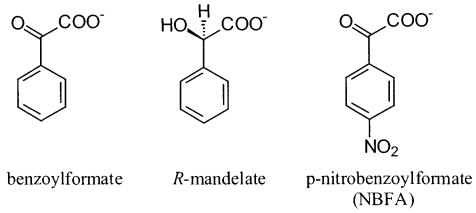

benzoylformate *R*-mandelate p-nitrobenzoylformate (NBFA)

† This research was supported at Purdue University by NSF Grant 9733552-MCB and by David and Lucille Packard Foundation Fellowship 99-1463 (to M.S.H.), by NIH Grant GM-50380, by the Rutgers Busch Biomedical Fund, by the Rutgers Board of Governors Fund, by Roche Diagnostics Inc. (Indianapolis, IN), and by NSF Grant BIR94/13198 (to F.J.), and by NIH Grant GM-40570 (to G.L.K.).

* To whom correspondence should be addressed. Telephone: (765) 496-2928. Fax: (765) 496-1189. E-mail: mhasson@bragg.bio.purdue.edu.

‡ Purdue University.

§ Current address: Kilpatrick Stockton LLP, 1100 Peachtree, Atlanta, GA 30309-4530.

|| University of Michigan.

⊥ Rutgers, the State University of New Jersey.

[1] Abbreviations: AU, absorbance units; BFD, benzoylformate decarboxylase; BSA, bovine serum albumin; CD, circular dichroism; DMF, dimethylformamide; HLADH, horse liver alcohol dehydrogenase; I_1, first covalent reaction intermediate or 2-α-mandelyl-ThDP; I_2, second covalent reaction intermediate, enamine, or 2-α-carbanion; PAGE, polyacrylamide gel electrophoresis; PDC, pyruvate decarboxylase; PEG MME, polyethylene glycol monomethyl ester; POX, pyruvate oxidase; PMSF, phenylmethanesulfonyl fluoride; NBFA, *p*-nitrobenzoylformate; SDS, sodium dodecyl sulfate; ThDP, thiamin diphosphate; U, international units of enzymatic activity (micromoles per minute); WT, wild type.

10.1021/bi026490k CCC: $25.00
Published on Web 01/30/2003

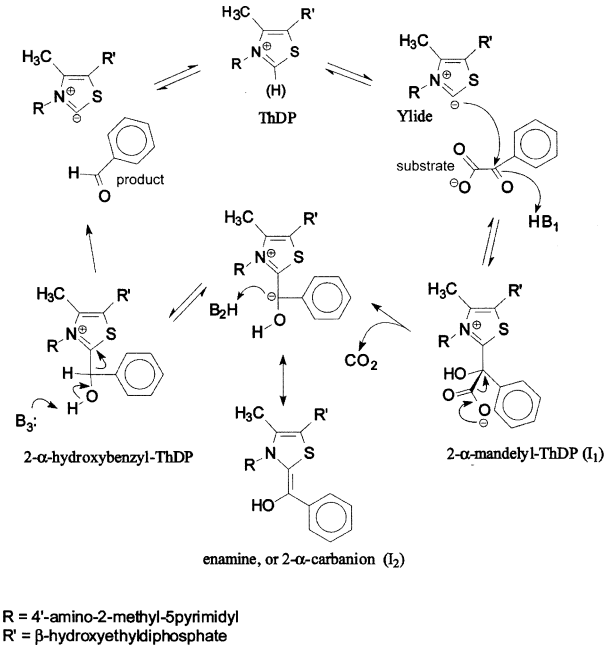

FIGURE 1: Postulated chemical mechanism for the BFD-catalyzed decarboxylation of benzoylformate.

aromatic nature of the BFD substrate allows for direct observation of the reaction intermediates by means of stopped-flow spectroscopy with a conservatively modified substrate *p*-nitrobenzoylformic acid (*11*).

The mechanism suggested for ThDP-dependent catalysis by benzoylformate decarboxylase (*9*, *12*−*14*), similar to that of related enzymes, is shown in Figure 1. In the initial step, the C4′ imino group of ThDP abstracts a proton from the C2 atom of the thiazolium ring, resulting in the formation of an ylide (*15*, *16*). The ylide attacks the carbonyl of the substrate to form the first tetrahedral intermediate, 2-α-mandelyl-ThDP. Decarboxylation of 2-α-mandelyl-ThDP results in the enamine intermediate (*17*−*20*). Protonation of the enamine provides a second tetrahedral intermediate, 2-hydroxybenzyl-ThDP. Finally, benzaldehyde is eliminated with the assistance of an enzymic base (*12*).

Examination of the known three-dimensional structures of ThDP-dependent enzymes (BFD, PDC, POX, transketolase, pyruvate:ferredoxin oxidase, and the pyruvate dehydrogenase multienzyme complex E1 component) suggests which active site residues are likely to participate in catalysis (*9*, *21*−*34*). While the overall architectures of the enzymes are closely related, it is surprising to see that none of the active site residues, except those directly bound to the cofactor or metal ion, are well-conserved. The differences in the residues seem to support the suggestion that it is the cofactor, its conformation and its environment, that supplies much of the catalytic effect (*18*) and that the individual residues are less important. It is possible that different residues are required simply to protect the intermediates from side reactions (*35*). Comparison of the roles of the residues in the different family members will improve our understanding of the nature of the active sites, their enzymology, and their evolution.

Enzymatic analysis of several yeast PDC active site mutants has allowed functional assignments for some of the active site residues, including two histidines and an aspartic acid (*36*−*41*). In addition, the X-ray structure of the substrate analogue pyruvamide, bound in the active site of PDC, hints at the positioning of the substrate pyruvate (*42*). Like PDC, BFD contains two active site histidines, which in the case of BFD are H70 and H281 (*9*). However, in BFD, the histidines are located on different subunits, whereas in PDC, they are adjacent in the protein sequence. Yet despite the difference in the origin of the histidines, the imidazole rings occupy similar positions relative to the ThDP cofactor. The active site aspartate (D28) of PDC provides a hydrogen bond to pyruvamide (*42*) and in BFD is replaced with a serine (S26). It would appear therefore that these residues, as well as the two histidine residues, may play similar roles in BFD and PDC (*9*).

Here we report the structure of BFD complexed with an inhibitor (*13*), (*R*)-mandelate. The structure suggests that, at a minimum, S26 is likely to assist in the binding of benzoylformate and confirms earlier suggestions that H70 and H281 may be positioned to act as catalytic acids and/or bases (*9*). To further explore the role of these residues, we prepared the H70A, H281A, and S26A mutants and carried out steady-state kinetic analyses. In addition, we used stopped-flow spectroscopy to observe directly the first two intermediates in the decarboxylation reaction catalyzed by wild-type (WT) BFD and each of the mutants. This technique has been used in the past to study ThDP-dependent catalysis by yeast PDC (*19*, *20*). Recently, it has been successfully applied in investigating the mechanism of BFD (*11*). The combined use of X-ray crystallography, site-directed mutagenesis, steady-state kinetics, and stopped-flow spectroscopy has allowed us to suggest roles for several amino acid residues in the BFD active site.

MATERIALS AND METHODS

Reagents. ThDP, benzoylformic acid, BSA, Gly-Gly, and NADH were purchased from Sigma. (*R*)-Mandelate and HLADH were purchased from Fluka. Piperazine and PEG MME 2000 were obtained from Aldrich. BSA, HEPES, and Tris were purchased from Midwest Scientific. Sodium and potassium phosphate, ammonium sulfate, sodium citrate, sodium and potassium hydroxide, and hydrochloric and acetic acid were all obtained from Mallinckrodt. Water was purified with a Nanopure system (Barnstead). All other chemicals that were used were of the highest available purity. *p*-Nitrobenzoylformic acid was available from a previous study (*11*). All solutions used for protein crystallization were filtered through 0.22 μm syringe filters (Midwest Scientific) and stored in sterile polypropylene tubes.

BFD Expression and Purification. The expression and purification of BFD (*10*, *11*) and construction of the BFD H70A mutant are described elsewhere (*11*). All mutants were prepared using *Pfu* DNA polymerase and the QuikChange site-directed mutagenesis kit (Stratagene, La Jolla, CA). The mutants were constructed using pBFDtrc (*43*) as the DNA template. The forward primers used for the mutagenesis are shown below with the mutated codons underlined and with the lowercase letters indicating a base change from the wild type: S26A, 5′-GCAATCCTGGCgCGAACGAGCTCCC-3′; and H281A, 5′-GTTCCGTTACgcCCAATACGAtCCAG-GTCAATATC-3′.

For BFD H281A, in addition to creating the histidine to alanine mutation, an additional silent mutation was intro-

duced which resulted in the loss of a *Psh*AI restriction site. Following mutagenesis, the template DNA was removed by treatment with *Dpn*I and the remaining PCR products were transformed into *Escherichia coli* strain XL1-Blue (Stratagene). Single colonies were picked, and their DNA was isolated and screened for the desired mutation by restriction analysis using *Psh*AI (H281A) or by sequencing (S26A). In both cases, the fidelity of the PCR amplification and the presence of the mutation were confirmed by sequencing. Plasmids containing the mutated BFD were selected and denoted pKKBFDH281A and pKKBFDS26A, respectively. These plasmids were used to transform *E. coli* M15[pRep7] (Qiagen) and single colonies chosen for the expression of the mutant BFD. Following purification using published methods (*11*), the WT and mutant proteins were analyzed by electrospray mass spectroscopy. The mass differences found between the proteins corresponded to the amino acid substitutions.

Protein Crystallization. Protein concentrations were determined with a Bradford assay (*44*) using BSA as a standard. The purified protein solutions contained 20−50 mg/mL BFD, 15 mM HEPES (pH 7.0), 0.2 mM ThDP, and 0.1 mM $MgCl_2$. All crystals were grown by the hanging drop vapor diffusion method (*45*). Costar 24-well plates, with 15 mm glass cover slides (Fisher) siliconized in-house with Prosil (Hampton Research), were used for protein crystallization. Initial conditions for crystallization were found through sparse matrix sampling with the Crystal Screen II (Hampton Research). After optimization, the well solution contained 20−22% PEG MME 2000, 100 mM sodium citrate (pH 5.2−5.6), 0.15−0.2 M $(NH_4)_2SO_4$, and 10 mM (*R*)-mandelate. Before equilibration, the drops contained 2−4 μL of well solution and 2−4 μL of the inactivated BFD solution. After the hanging drops were set up, the plates were equilibrated at 20 °C until crystals appeared (3−14 days). The drops that failed to produce protein crystals were seeded with microcrystals (*45*), which resulted in the appearance of the crystals in ~30% of the seeded drops. The crystallization conditions described above gave rise to several different crystal forms. The type of the crystal lattice could be determined only after the collection of the diffraction data.

Prior to data collection, the crystals were transferred into a stabilizing solution of 20% PEG MME 2000, 15% glycerol, 100 mM sodium citrate (pH 5.4), 0.05 M $(NH_4)_2SO_4$, and 10 mM (*R*)-mandelate. The crystals were incubated in this solution for 10−20 min and then soaked in a series of four solutions containing increasing concentrations of glycerol and decreasing concentrations of ammonium sulfate in addition to the well solution components. The "soaking out" of ammonium sulfate was necessary for removal of the sulfate ion bound in the active site of BFD. A sulfate ion was present in the active site in the structures of BFD crystallized with the substrate analogues but not subjected to soaking. The crystals were incubated for 15−20 min in each of the intermediate solutions. The crystals were soaked for 1.5 h in the final soaking solution that contained 15% PEG MME 2000, 15% glycerol, 100 mM sodium citrate (pH 5.4), and 0.1 mM (*R*)-mandelate. The integrity of the crystals was monitored throughout soaking, and damaged crystals were discarded.

Data Collection and Structure Determination. The crystals were mounted onto a cryoloop and flash-cooled to 100 K in a stream of nitrogen (Oxford Cryosystems). Data collection was carried out at 100 K on an *R*-AXIS IV image plated detector (Molecular Structure Corp.) using 0.3 mm collimated monochromatized Cu Kα radiation from a Rigaku RU-200 rotating anode generator (50 kV and 150 mA). The structure was determined from a data set collected from a single crystal at a crystal-to-detector distance of 200 mm.

Table 1: Data Collection and Refinement Statistics

space group	$P2_1$ ($\beta = 97°$)
a (Å)	135
b (Å)	210
c (Å)	163
no. of BFD monomers per ASU	16
high-resolution limit (Å)	2.8
no. of total reflections ($I/\sigma_I > 1$)	561773
no. of unique reflections ($I/\sigma_I > 1$)	206940
completeness (%) ($I/\sigma_I > 1$)	94
R_{sym} (%)	7.3
completeness (%) ($I/\sigma_I > 1$) (2.8−2.9 Å)	76
R_{sym} (%) (2.8−2.9 Å)	18.7
average I/σ_I	9.1
rmsd for bond lengths (Å)	0.007
rmsd for bond angles (deg)	1.37
avg *B* factor (Å^2)	19
avg protein *B* factor (Å^2)	19
avg ThDP *B* factor (Å^2)	19
avg (*R*)-mandelate *B* factor (Å^2)	26
avg water *B* factor (Å^2)	17
final *R* factor (%)	20
final R_{free} (%)	22

The HKL software suite (*46*, *47*) was used to index and scale the data in space group $P2_1$. After the first round of processing, the data to 2.8 Å resolution where $I/\sigma_I \geq 1$ were chosen for all further analysis and were reprocessed. The software package AMoRE (*48*), part of the CCP4 program suite (*49*), was used to carry out molecular replacement, using the coordinates of the tetramer of the BFD crystal structure (space group *I*222) as a starting model (*9*). The initial molecular replacement solutions were used to generate a model of the asymmetric unit, using coordinates of a BFD monomer of a different crystal form (space group $P2_12_12$) obtained under identical conditions. Although only sulfate was bound in the active site of the $P2_12_12$ crystal structure, the model was used to determine this (*R*)-mandelate-bound structure because the crystallization conditions were similar. To improve the phase information, the program Dm, a component of the CCP4 program suite, was used to perform the 16-fold noncrystallographic averaging using operators generated with the LSQ facility of the molecular modeling program O (*50*). The modified data were used in the refinement. Rigid body, positional, and individual *B* factor refinement with noncrystallographic symmetry restraints (Table 1) were carried out on each of the three domains of the monomer using the program XPLOR (*51*), followed by CNS (*52*), with 10% of the data randomly excluded from minimization for calculation of R_{free}. Using XPLOR, the $2F_o - F_c$ and $F_o - F_c$ electron density maps were subsequently averaged 16-fold using the programs MAMA and AVE, while in CNS, the averaging was done in the program itself. Electron density maps were examined with the program O. A model of (*R*)-mandelate was included in each of the active sites for the second round of refinement, using relevant data files from the HIC-Up database (*53*). Water molecules were incorporated into the model before

the third round of refinement. Following the third round of refinement, the electron density maps were contoured at a negative level and examined to ensure that none of the water molecules that were included resulted in negative peaks in the map. In the final structure, no residues are in the disallowed regions of a Ramachandran plot, and three residues of each monomer, S71, H281, and P447, are in generously allowed regions. Atomic coordinates and structure factors have been deposited in the Protein Data Bank as entry 1MCZ.

Active site drawings were generated with Ribbons (*54*), povscript (D. Peisach, peisach@mit.edu, and T. Fenn, fenn@brandeis.edu), molscript (P. Kraulis, www.avatar.se/molscript), povray (www.povray.org), and Adobe Photoshop (Adobe Systems Inc.).

Circular Dichroism (CD) Spectroscopy. Near-UV CD spectra were recorded at 20 °C on a JASCO-810 spectropolarimeter. The spectra were recorded over a wavelength range of 250−320 nm. Quartz cells with a path length of 1 cm were used. Spectral parameters were as follows: (a) time constant of 2 s, (b) scan speed of 100 nm/min, (c) scanning increment of 0.1 nm, and (d) spectral bandwidth of 1 nm. Before the CD spectra had been recorded, the buffers of the WT and mutant BFD protein solutions were exchanged to 0.1 M potassium phosphate (pH 6.7) in an Amicon Microcon microconcentrator. The protein concentration was adjusted to 1−1.4 mg/mL.

Determination of Kinetic Parameters. All steady-state kinetic studies were carried out using benzoylformate, the natural substrate. A coupled enzymatic assay (*13*) employing horse liver alcohol dehydrogenase (HLADH) was used to obtain the initial velocity data used in the determination of the kinetic parameters. Protein concentrations were determined with the Bradford assay (*44*) using BSA as a standard. Each initial velocity measurement was performed in triplicate. Determination of kinetic parameters was performed at 20 °C in 36 mM Gly-Gly and 36 mM piperazine buffer (final concentration in the assay). Kinetic parameters were calculated per monomer using a molecular mass of 56 200 Da. The assay mix contained 0.1−0.5 unit/mL HLADH, 0.5 mM ThDP, and 0.2 mM NADH. The reaction was initiated by the addition of enzyme. The decrease in absorbance at 340 nm was measured on a Perkin-Elmer spectrophotometer equipped with a temperature-controlled cell holder. The initial velocity was directly proportional to the concentration of BFD in the assay under all the conditions that were studied.

Stopped-Flow Experiments. The stopped-flow experiments were performed using the substrate analogue (*11*) *p*-nitrobenzoylformate (NBFA). The experiments were performed in a stopped-flow instrument (Applied Photophysics) under pseudo-first-order conditions (2.5 mM NBFA and 40 μM enzyme). The first covalent intermediate of the reaction (I_1, assigned to 2-α-*p*-nitromandelyl-ThDP) was monitored at a wavelength of 620 nm and the second intermediate (I_2, assigned to the enamine) at 420 nm (*11*). All experiments were performed at 25.6 °C in 100 mM sodium HEPES (pH 7.0).

Steady-State Kinetic Data Analysis. Initial velocity data were fitted to the Michaelis−Menten equation (eq 1) using the program KaleidaGraph (Synergy Software). Dixon plots were used to show that (*R*)-mandelate was a competitive inhibitor of WT and mutant BFD (*55*). Initial velocity data were fitted to eq 2 to determine competitive inhibition parameters.

$$v = \frac{V_{max}[S]}{K_m + [S]} \quad (1)$$

$$v = \frac{V_{max}[S]}{K_m\left(1 + \frac{[I]}{K_i}\right) + [S]} \quad (2)$$

RESULTS

Overall Structure of the BFD−(R)-Mandelate Complex. The unliganded structure of BFD was determined from crystals of space group *I*222, grown at pH 8.5 at high concentrations of calcium ions (*9*, *10*). In past experience, these conditions precluded binding anything but water in the active site, so alternative conditions were sought. Cocrystallization of BFD with (*R*)-mandelate at pH 5.4, in the presence of ammonium sulfate rather than calcium chloride, gave rise to several different crystal forms. When diffraction data were collected from crystals soaked in substrate, a compact, high-density peak was found in the active site. We attribute this peak to a sulfate ion, first because the crystallization solution contained relatively high levels of ammonium sulfate (≥0.15 M) and second because BFD is known to be catalytically inactive in the presence of sulfate ions. To observe (*R*)-mandelate bound to the active site, it was necessary to soak the crystals in a series of solutions containing increasing concentrations of glycerol and decreasing concentrations of ammonium sulfate. Only the crystal form reported here, of space group $P2_1$, showed electron density in the active site that could be attributed to the bound inhibitor.

The structure of (*R*)-mandelate-bound BFD was determined to 2.8 Å resolution (Table 1). The final model includes residues 2−524 in each of the 16 monomers (a total of 8368 residues in four tetramers) in the asymmetric unit. Each of the four tetramers contains four ThDP molecules, four Mg^{2+} ions bound to ThDP, and two Mg^{2+} ions shared by the same residues in two monomers. Each monomer contains 103 or 104 equivalent water molecules, giving a total of 1656 water molecules. The electron densities of the polypeptide chain and the cofactor are well-defined. In the initial $F_o - F_c$ maps (Figure 2A), the (*R*)-mandelate molecule can be placed in an extra patch of electron density in the active sites, with its position confirmed by close examination of nonaveraged maps. The electron density accommodating the aromatic ring of (*R*)-mandelate is the correct shape, but is marginally smaller than expected in the final $2F_o - F_c$ map. It is possible that a smaller molecule, possibly a sulfate ion, may replace (*R*)-mandelate in some of the monomers.

The structures of unliganded BFD (*9*) and the (*R*)-mandelate-bound enzyme are quite similar, with an overall rmsd of the C_α atoms in the two structures of 0.26 Å. The largest differences are correlated with segments of high *B* factor and are consistent with the expected coordinate error. The helix containing residues 460−470 has the highest average *B* factor in both structures. Noncrystallographic symmetry restraints were imposed on the 16 monomers in the (*R*)-mandelate asymmetric unit compared to one molecule in the *I*222 asymmetric unit. However, two positions of the

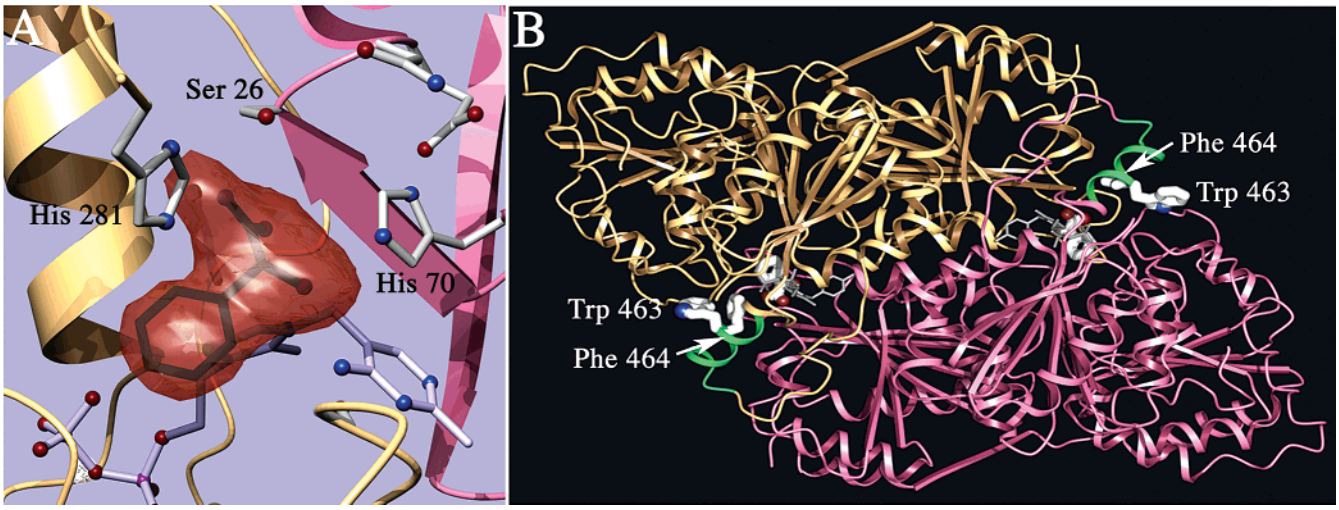

FIGURE 2: Electron density showing (*R*)-mandelate in the active site. (A) The initial $F_o - F_c$ map of monomer A (yellow) and of its partner in constructing active sites, monomer B (pink), is shown. (B) A view of monomers A and B looking down a pseudo-2-fold axis shows the movement of helix formed by residues 460−470 (green). The side chains of F464 and W463 flip outward in the active site on the right, and inward on the one on the left. The structures of (*R*)-mandelate and ThDP are shown in white and gray, respectively.

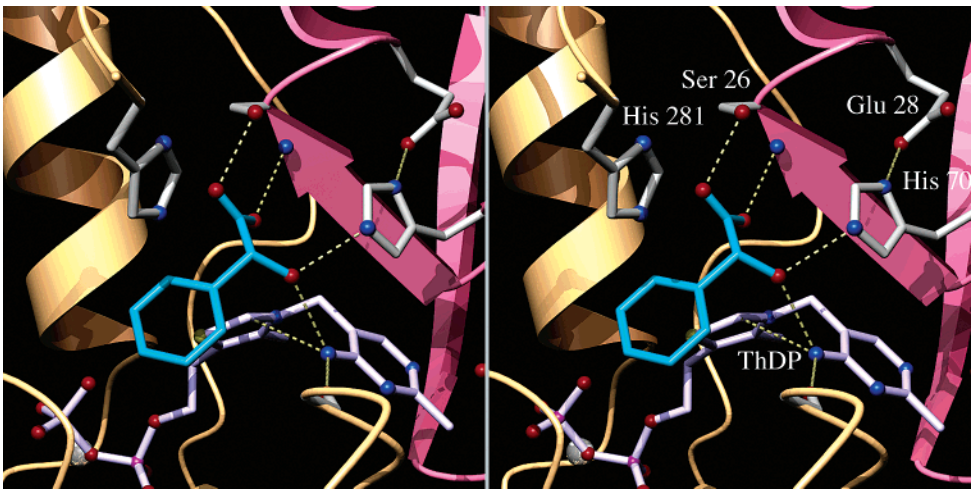

FIGURE 3: Stereoview of the active site of monomer A showing <3 Å contacts between (*R*)-mandelate and the enzyme. The carboxylate of (*R*)-mandelate forms two hydrogen bonds with S26, one with the hydroxyl group on the side chain and the other with the amide nitrogen on the main chain. The C_α OH group forms hydrogen bonds with both N1′ of ThDP and N4 of H70. The other nitrogen on the imidazole ring of H70 forms a hydrogen bond with E28, possibly forming a proton relay system.

helix from residue 460 to 470 in seven of the 16 monomers were added to the symmetry restraints in later rounds. In seven of the eight pairs of monomers that form the active sites, both conformations of the helix are present (Figure 2B). In monomers A and D in the first tetramer, E and F in the second, I and J in the third, and M in the fourth, the helix of residues 460−470 has a position similar to that in the unliganded structure (*9*). The movement of the helix results in distinctly different conformations of two residues, W463 and F464. In particular, in one conformation the phenyl ring of F464 is within 4 Å of (*R*)-mandelate, and in the other, it is more than 5.5 Å away. The electron density map in the active site region suggests that (*R*)-mandelate may be bound more securely when the position of the helix is similar to that in the original structure. Two monomers that have the helix positioned in this manner are always neighboring in the tetramers, each sharing active sites with monomers in which the mobile helix is in the alternate conformation.

(R)-Mandelate Binding Site. A stereoview of the binding mode of (*R*)-mandelate is shown in Figure 3. As expected, the inhibitor lies in the proximity of the thiazolium ring of the ThDP cofactor. (*R*)-Mandelate makes hydrogen bonds to the hydroxyl of S26 through its carboxylate group and, through its hydroxyl group, to a nitrogen atom on the side chain of H70 and the 4′-imino group of ThDP. H281, the other potential active site acid−base catalyst, is located less than 3.5 Å from the aromatic ring and a carboxylate oxygen of the inhibitor. The remaining interactions used to position the inhibitor appear to be of the van der Waals type.

Steady-State Kinetic Studies. On the basis of the crystallographic evidence described above, S26, H70, and H281 might be expected to play a significant role in the catalytic mechanism of BFD. Further, these residues are analogous to those implicated by mutagenic studies as being important catalytic residues in PDC (*36*−*41*). The mutants S26A, H70A, and H281A were prepared and overexpressed in *E. coli*. A soluble enzyme was obtained in all cases, and was

Table 2: Steady-State Kinetics of Benzoylformate Decarboxylation by Wild-Type and Mutant BFD[a]

	K_m (mM)	k_{cat} (s^{-1})	k_{cat}/K_m (mM^{-1} s^{-1})	$K_i^{(R)\text{-mandelate}}$ (mM)[b]
WT	0.37 ± 0.02 (1)	241 ± 4 (1)	651 ± 38 (1)	1
H70A	1.92 ± 0.1 (5)	0.07 ± 0.02 (3394)	0.037 ± 0.019 (17595)	40
H281A	1.68 ± 0.3 (4)	1.41 ± 0.19 (171)	0.84 ± 0.19 (775)	40
S26A	8.62 ± 1.2 (23)	4.45 ± 0.62 (54)	0.52 ± 0.08 (1252)	100

[a] Reactions were carried out in 50 mM Gly-Gly and 50 mM piperazine buffer at pH 7.0 ± 0.2. The K_i data for (*R*)-mandelate were obtained at pH 6.5. In parentheses is the fold change from the WT value. The errors reported for k_{cat} and K_m are the errors of the fit of the experimental data to the Michaelis−Menten equation (eq 1), where each data point was determined in at least triplicate. The errors reported for k_{cat}/K_m were calculated using standard error propagation formulas. [b] Inhibition parameters for (*R*)-mandelate were determined by using eq 2 at benzoylformate concentrations ranging from 1 to 5 mM. Each data point was determined in triplicate. Reported parameters are the average of these determinations.

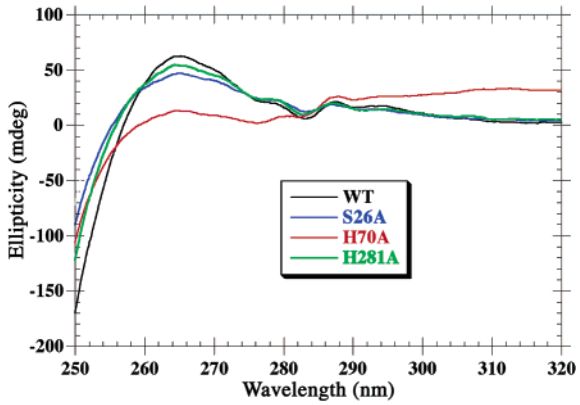

FIGURE 4: Near-UV CD spectra of WT BFD and S26A, H70A, and H281A. Spectra were obtained in 0.1 M potassium phosphate buffer at 20 °C and pH 6.7, at an enzyme concentration of 1−1.4 mg/mL.

purified using the methodology described for the WT enzyme (*11*). The near-UV CD spectrum of WT BFD (Figure 4) exhibits the shape characteristic of ThDP-dependent enzymes, with the maximum originating from the cofactor at 265 nm (*56*, *57*). The spectra of the S26A and H281A mutants are similar to that of the WT enzyme, suggesting that the tertiary structure of the protein is not disturbed by these mutations. Interestingly, the near-UV CD spectrum of the H70A mutant differs somewhat from that of the WT. However, preliminary experiments suggest that there are no significant differences between the X-ray structures of the WT and H70A mutant (data not shown). Circular dichroic spectra can be very sensitive to small changes in protein−cofactor interactions (*58*), and it is possible that the disturbances in the near-UV CD spectrum of H70A may be indicative of the proximity of the side chain of H70 to the cofactor in the active site.

The Michaelis−Menten steady-state parameters for the BFD mutants are shown in Table 2. The K_m values for the two histidine mutants are slightly higher than the K_m value for the WT enzyme, while the K_i values for the binding of (*R*)-mandelate increased ~40-fold in both cases. In contrast, the S26A mutant exhibited an even greater decrease in the affinity for both the substrate and (*R*)-mandelate. All mutants had values of k_{cat} significantly lower that of the WT, with the H70A mutant showing the greatest loss of activity (almost 3500-fold). Taken together, these results confirm the suggestion that these residues would be catalytically important and suggest that S26, in particular, would play a major role in substrate binding.

Stopped-Flow Kinetics. All stopped-flow experiments were performed using *p*-nitrobenzoylformate (NBFA, Chart 1), a chromophoric substrate shown previously to be quantitatively converted to the *p*-nitrobenzaldehyde product (*11*). Given the quantitative conversion and the rate constants described below, it is very unlikely that possible cofactor destruction (*35*) is present in the enzyme-catalyzed reaction. The K_m value for NBFA is 0.154 mM, and the enzyme turns over this substrate very slowly with a k_{cat} value of <0.04 s^{-1} (*11*). Product release is the rate-limiting step in the reaction (*11*). In the experiments described here, the concentration of NBFA was considerably in excess compared to that of the enzyme. This has the advantage of maintaining an effectively constant substrate concentration and allows the observation of the first two intermediates under single-turnover conditions. Although the presence of the nitro group in the substrate may change the relative kinetic significance of the reaction steps, the nitro substrate and the natural substrate seem to react identically up to the enamine stage (ref *11* and Table 3, for example, here). While the steps after enamine formation are slower using NBFA, the role of the acid−base amino acids could still be deduced, because the nitro group is not expected to participate in ionic interactions. In addition, the postdecarboxylation phase is rate-limiting with the natural substrate as well (*13*, *14*). Thus, NBFA appears to be a suitable probe of the role of the active site residues.

Observations for the reaction catalyzed by the wild-type enzyme are similar to previously reported data and can be used to analyze the steps of the reaction (*11*). The amount of 2-α-*p*-nitromandelyl-ThDP (I_1, a charge transfer band at $\lambda_{max} = 620$ nm) increased over the first 10 ms of the reaction and was depleted completely within 100 ms (Figure 5A). Concomitantly, there was an increase in the concentration of the enamine intermediate (I_2, $\lambda_{max} = 420$ nm; Figure 5B). The enamine was then slowly depleted (Figures 5C and 6). If a mutation slows the appearance of I_1, it suggests that the wild-type residue is important in the formation of the first covalent intermediate, 2-α-*p*-nitromandelyl-ThDP. Changes in the rate of the decrease in the amount of I_1 and in the increase in the amount of I_2 indicate that the mutation affects the decarboxylation step, while superficially, changes in the rate of the decrease in the amount of I_2 would appear to indicate the effect of the mutation on the rate of the protonation of the enamine to form 2-α-*p*-nitrohydroxybenzyl-ThDP. However, mathematical analysis suggests that, for the reaction of *p*-nitrobenzoylformate with WT BFD, the decrease in the amount of I_2 can only be explained using a combination of two separate linear rates (Figure 6). This suggests the resolution of the two consecutive steps in the postdecarboxylation part of the reaction, i.e., protonation of the enamine and product (*p*-nitrobenzaldehyde) release.

Table 3: Summary of Rate Constants Deduced from Stopped-Flow Data for WT BFD and Mutants with NBFA as the Substrate at pH 7.0 and 25.6 °C[a]

$$E + S \rightleftharpoons E^*S \overset{k_1}{\rightleftharpoons} E^*\text{mandelyl-ThDP} \overset{k_2}{\rightarrow} \text{Enamine} \overset{k_3}{\rightarrow} E^*\text{hydroxybenzyl-ThDP} \overset{k_4}{\rightarrow} E + P$$

$$\downarrow CO_2$$

	k_1	k_2	k_3	k_4
WT	238.3 ± 1.51	52.9 ± 0.173	0.0052 ± 0.00011	0.52 ± 0.043
H70A	0.573 ± 0.026	($\gg k_1$)[b]	0.0054 ± 0.00013	ND
H281A	4.83 ± 0.05	15.78 ± 0.09	(2.46 ± 0.134) × 10^{-6} [c]	0.55 ± 0.014
S26A	2.72 ± 0.0187	($\gg k_1$)[b]	(1.15 ± 0.175) × 10^{-6} [c]	ND

[a] All rate constants (k_1−k_4) are in units of inverse seconds. Each rate constant is the overall rate of a particular step of the reaction, as follows: k_1, formation of 2-α-*p*-nitromandelyl-ThDP; k_2, formation of the enamine; k_3, formation of 2-α-*p*-nitrohydroxybenzyl-ThDP; and k_4, formation of the product. ND means the value could not be determined. [b] Although the value of k_2 is unavailable, it is expected to be much greater than k_1.[c] Units are absorbance$_{420}$ per second.

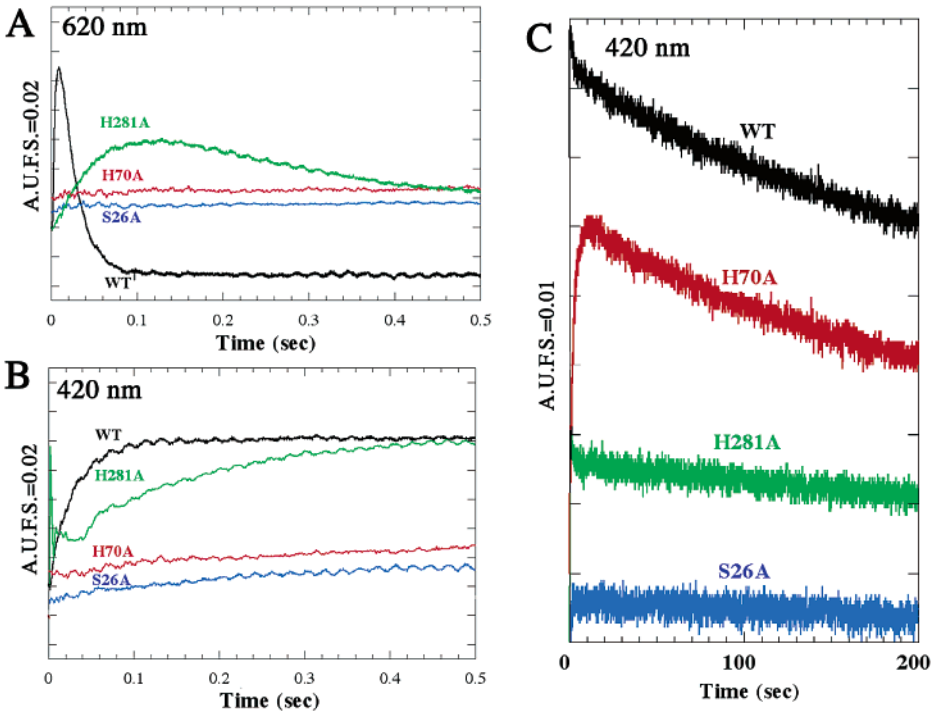

FIGURE 5: Absorbance at 620 (A) and 420 nm (B and C) as a function of time after mixing BFD (40 μM) with 2.5 mM *p*-nitrobenzoylformate (NBFA) in 100 mM sodium HEPES at pH 7.0 and 25 °C. The starting *y* value of each curve is arbitrary.

All mutants showed some effect on the rate of formation of I_1 (Figure 5A), but only the H281A mutant exhibited the fast decrease in I_2 observed with WT BFD (Figure 6B). Given the relative distance of H281 from the hydroxyl group of (*R*)-mandelate (Figure 3), it is unlikely that H281 participates in proton abstraction from the C_α OH group to release the *p*-nitrobenzaldehyde product. Therefore, we have tentatively assigned the fast descending exponent to the last step in the catalytic cycle. By a process of elimination, we then conclude that the slower phase of the decrease in the amount of I_2 must correspond to the protonation of the enamine and, with the NBFA substrate, this is the rate-limiting step.

A single-exponential decrease in the level of I_2 was seen with the S26A and H70A mutants (Figure 6B). This suggests that, for these mutants, the breakdown of 2-α-*p*-nitrohydroxybenzyl-ThDP is slower than the protonation of the enamine. The rate constants shown in Table 3 were obtained using relaxation kinetic theory (*40*, *59*) as described previously (*11*). In broad terms, the stopped-flow results suggest that H70 plays a significant role in the formation of the 2-α-*p*-nitromandelyl-ThDP intermediate (I_1) and in product release, but not in the protonation of the enamine intermediate (I_2). H281, on the other hand, plays its major role in enamine protonation but has little effect on product release. Finally, S26 is implicated in all three of these steps, that is, the formation of I_1, enamine protonation, and product release.

DISCUSSION

The initial structure of BFD revealed an unexpected diversity of active site residues among the family of ThDP-dependent enzymes, and in particular between two decarboxylases, BFD and PDC (*9*). It was suggested that S26, H70, and H281 of BFD could play somewhat similar roles in the catalytic mechanism as an aspartate and two histidines in the active site of both *Zymomonas mobilis* and *Saccharomyces cerevisiae* PDC. To explore this hypothesis, we designed and carried out experiments to obtain both structural and kinetic data that might delineate the role of these three residues in BFD.

In the first phase of our study, we determined the structure of a competitive inhibitor, (*R*)-mandelate (*13*), bound to BFD.

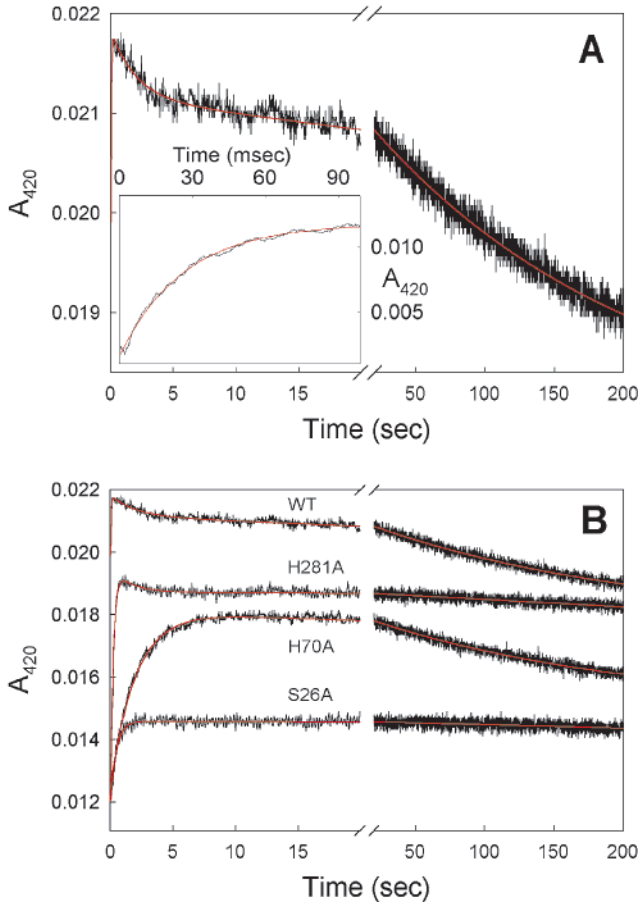

FIGURE 6: Progress curve at 420 nm for the reaction of NBFA with WT BFD (A) and active site mutants (B). Conditions are the same as in Figure 5. An initial one-exponential increase (A, inset; rate constant of 37.8 s^{-1}) is followed by a two-exponential decrease (rate constants of 0.51 and 0.0052 s^{-1}).

The solution of the structure of the BFD−(*R*)-mandelate complex was enhanced through the use of 16-fold averaging in the map and noncrystallographic symmetry constraints. Inspection of the structure of the complex suggests that, with one striking difference, the four tetramers in the asymmetric unit have similar conformations. The helix formed by residues 460−470 is the only part of the structure that required two separate orientations, involving movement of the entire helix and radically different conformations of two residues, W463 and F464, which regulates the contact between F464 and (*R*)-mandelate (Figure 2C). In seven of the eight pairs of monomers that form the active sites, both conformations of the helix are present. The two monomers that share the same conformation of the helix are those that are not in the same dimer, but interact closely in the tetramer, reminiscent of the dimeric interactions in yeast PDC (*42*, *60*). In the latter, the comparison of the active and inactive monomers reveals a readily apparent movement of one domain relative to the others. Such a movement is not obvious in BFD. It is conceivable that the position of the helix in BFD may correlate with the binding of the substrate, but a structure at higher resolution that does not require noncrystallographic structural averaging is necessary to confirm this. We have previously predicted the alternation of active sites reactivity in a functional dimer of BFD based on kinetic studies (*11*). Together, the structural and biochemical experiments suggest that BFD may share the property of alternation of active sites reactivity within a functional dimer (*61*).

While (*R*)-mandelate can be viewed as an analogue of benzoylformate, the fact that C2α is sp^3 rather than sp^2 hybridized suggests that it may be better viewed as an analogue of the 2-α-mandelyl-ThDP intermediate (*13*). Even that view is somewhat contentious, as the mandelate does not form an adduct with ThDP, but at least the hybridization at C2α is correct. In any event, there is relatively little difference in the binding affinities of benzoylformate and (*R*)-mandelate (Table 2), so it is not unreasonable to use the latter to screen for residues likely to be involved in substrate binding or catalysis. Not surprisingly, as shown in Figure 3, the inhibitor was found to lie adjacent to the thiazolium ring of the ThDP cofactor, making hydrogen bonds to S26 and H70 as well as to the 4α′-imino group of the cofactor. H281 was also located within 3.5 Å of the inhibitor, suggesting that any or all of these residues are likely to be active participants in the catalytic cycle.

Histidine 70. The replacement of H70 with alanine has a pronounced effect on the overall rate of the reaction, with k_{cat} being reduced by more than 3 orders of magnitude. However, this effect on rate is not accompanied by a similar effect on substrate binding, as evidenced by an only 5-fold increase in K_m for benzoylformate and a 40-fold increase in K_i for (*R*)-mandelate (Table 2). The K_m for benzoylformate is also its K_d (*13*), and as a consequence, the K_i values for (*R*)-mandelate can be directly compared to the corresponding K_m value for benzoylformate. Phenylacetate, in which the keto group of benzoylformate is replaced with a methylene, binds approximately 100-fold less tightly to WT BFD (*13*). This indicates the importance of the hydrogen bond formed between the α-keto group and the enzyme. The binding data imply that H70 is better positioned to bind to the tetrahedral intermediate (2-α-mandelyl-ThDP) than to the substrate, while the k_{cat} data implicate H70 in a significant role both pre- and postdecarboxylation.

The BFD−inhibitor structure shows that H70 forms a hydrogen bond to the α-OH group of (*R*)-mandelate and a second hydrogen bond to E28 (Figure 3). The structure suggests that H70 assists in the attack of the ylide, resulting in the formation of 2-α-mandelyl-ThDP, by either positioning the substrate appropriately or, with the help of the 4′-imino group of ThDP, protonating the carbonyl oxygen of benzoylformate (i.e., H70 is HB_1 in Figure 1). As suggested by the kinetic studies, it may also accept a hydrogen bond to stabilize the intermediate. Further, it offers the possibility that H70 is the base (B_3, Figure 1) that removes the proton from 2-α-hydroxybenzyl-ThDP to promote the release of benzaldehyde. Finally, examination of the structure gives rise to the possibility that the ionization state of H70 is mediated by E28; that is, H70 and E28 may form part of a proton relay.

Comparison of the stopped-flow kinetic profile of the H70A mutant with that of WT BFD (Figure 5A) reveals that the early increase in absorbance at 620 nm, attributed to the first covalent reaction intermediate, 2-α-*p*-nitromandelyl-ThDP (*11*), disappears. If the H70A substitution dramatically decreases the rate of appearance of I_1 without changing the rate of conversion of I_1 to I_2, the amplitude of I_1 would decrease. For example, using the value of 0.5 s^{-1} as the rate of 2-α-*p*-nitromandelyl-ThDP formation for the H70A

mutant (Table 3) and setting its decarboxylation rate constant equal to that of the WT (53 s^{-1}, Table 3) lead to an estimated amplitude that is 2 orders of magnitude smaller for the I_1 intermediate. It should also be noted that the observed rate of appearance of I_2 cannot exceed the slower rate of 2-α-*p*-nitromandelyl-ThDP formation. In WT BFD, the rates of both 2-α-*p*-nitromandelyl-ThDP formation and decarboxylation exhibited dependence on substrate concentration (*11*), preventing an unequivocal assignment of the apparent rate constant of the mutants. The presence of I_1 in WT BFD becomes most apparent between pH 6 and 7, suggesting that the electron donor contributing to the charge transfer band may be a histidine (*11*). If the imidazole ring of H70 is an essential contributor to the charge transfer band, there is a chance that removal of the histidine side chain would reduce the absorbance at 620 nm; i.e., the amplitude of I_1 would decrease. However, in the H70A mutant, as the amount of I_2 increases, the amount of I_1 also increases a small amount, suggesting rather that it is the reduced concentration of 2-α-*p*-nitromandelyl-ThDP that slows the rate of decarboxylation. The visibility of a small amount of I_1 emphasizes that decarboxylation is still a partially rate-limiting step, just as in WT BFD.

Both implied functions of H70 in the formation of 2-α-*p*-nitromandelyl-ThDP, i.e., ensuring the correct orientation of the substrate and contributing to the protonation of the carbonyl oxygen of the substrate, require H70 to be protonated prior to substrate binding. If the proton is transferred from H70 to the alkoxide, H70 would be in its neutral ionization state in the presence of I_1 and able to accept a hydrogen bond from the intermediate. This deduction is supported by the effect of pH on I_1, which suggests that the participating histidine is indeed neutral at this stage (*11*). If H70 is protonated prior to 2-α-*p*-nitromandelyl-ThDP formation and neutral during the decarboxylation step, we would expect a significant effect of the H70A substitution on the rate of 2-α-*p*-nitromandelyl-ThDP formation, but not on decarboxylation. As shown in Table 3, the H70A substitution slows the rate of formation (k_1) of 2-α-*p*-nitromandelyl-ThDP more than 400-fold. We suggest that the rate of decarboxylation (k_2) remains relatively unaffected, and certainly much higher than k_1, which would be consistent with the observation of low absorbance at 620 nm.

As described in the Results, the two consecutive steps in the postdecarboxylation part of the reaction, enamine protonation and product release (Figure 1), seem to be resolved in the stopped-flow kinetic results at 420 nm (I_2). The kinetic behavior of I_2 for WT BFD can be analyzed with a single-exponential increase, presumably representing enamine formation, followed by a two-exponential decrease (Figure 6A). The slow phase of the decrease has been attributed to the protonation of the enamine, while the fast stage has been assigned to the deprotonation of 2-α-*p*-nitromandelyl-ThDP and concomitant product release. The H70A mutant exhibited only a single phase for the decrease in the level of I_2 (Figure 6C) with a rate constant (k_3) similar to that of the WT enzyme. It would appear, therefore, that the H70A substitution has little effect on the protonation of the enamine and a considerable effect on the deprotonation of 2-α-*p*-nitromandelyl-ThDP.

In summary, we have assigned H70 the roles of protonation of the carbonyl oxygen of benzoylformate, thereby assisting the formation of 2-α-mandelyl-ThDP (HB_1, Figure 1), and removal of a proton from 2-α-hydroxybenzyl-ThDP (B_3, Figure 1) to allow the release of the product.

Histidine 281. Figure 3 shows that H281 is located close to the phenyl group and the carboxylate group of the inhibitor, suggesting it may play a part in binding the substrate or in stabilizing the formation of 2-α-mandelyl-ThDP. This was to some extent supported by the steady-state kinetics which showed that the H281A substitution increased the K_i of (*R*)-mandelate almost 40-fold while the K_m value for benzoylformate increased 4-fold. The k_{cat} value decreased 170-fold, suggesting that H281 is catalytically important, but not essential. In the stopped-flow experiments, the patterns of formation and breakdown of 2-α-*p*-nitromandelyl-ThDP (I_1) and the formation of the enamine (I_2) were similar to those observed for WT BFD. However, the rates of appearance of both I_1 and I_2 were approximately 1 order of magnitude slower with the H281A mutant than with the WT enzyme (Table 3), suggesting that the presence of H281 has a minor effect on the rates of 2-α-*p*-nitromandelyl-ThDP formation and its subsequent decarboxylation. As with the WT enzyme, the breakdown of I_2 was biphasic but the slower phase was much slower for H281A than its WT counterpart. The faster of the two phases had a rate comparable to the corresponding rate of WT BFD (k_4, Table 3). Taken together, the latter data imply that H281 is involved in the protonation of the enamine. As H281 is located a considerable distance from the enamine, this would require that the active site undergo a conformational change and adopt a more closed conformation. This is not unreasonable as H281 is located on a flexible loop (*9*), and such a conformational change has been proposed for *Z. mobilis* PDC where catalytically important histidine residues are located some distance from the cofactor (*36*). In summary, we conclude that H281 is important for the formation of 2-α-hydroxybenzyl-ThDP; i.e., it plays the role of HB_2 (Figure 1), plays a lesser role in the positioning of the substrate, and is not significant in the release of the product, benzaldehyde.

Serine 26. The K_i value for (*R*)-mandelate increases 100-fold for the S26A mutant (Table 2). Not surprisingly, S26 is found to hydrogen bond to both carboxylate oxygens of the inhibitor (Figure 3), suggesting that this residue may also perform a similar role in binding the substrate. Again, the steady-state kinetic data support this, with the K_m for benzoylformate increasing more than 20-fold. The k_{cat} value was also reduced, albeit not as markedly as those of the histidine mutants. In the stopped-flow studies, the formation of I_1 could not be observed with the S26A mutant, and the rate of I_2 formation was 1 order of magnitude slower than with the WT enzyme. The magnitude of this decrease falls somewhere between those for H70A and H281A (Table 3) and is consistent with S26 positioning the substrate for attack by the ylide and, potentially, for facilitating the expulsion of carbon dioxide. The progress curve for I_2 depletion was monophasic with the derived rate constant comparable to that observed for the slow phase with H281A (Table 3). While it is not readily apparent what role S26 may play in the protonation of the enamine, the sum of these observations suggests that S26 is important not only for substrate binding and decarboxylation but also for enamine protonation and benzaldehyde release.

Comparison with Pyruvate Decarboxylase. All known ThDP-utilizing enzymes are totally dependent on their cofactor, and all facilitate the same core reaction. Yet each must utilize this basic capability in a different manner to catalyze the specific reaction for which it has evolved. There is a general lack of conserved residues in the active site of ThDP-dependent enzymes, except for those bound to the cofactor. However, occasionally, some similarity seems to exist. For instance, it appears that the two decarboxylases PDC and BFD have histidine residues in the active site in similar relative positions with respect to the cofactor (*9*, *21*, *62*). There are now many examples of enzyme homologues in which residues playing the same catalytic role are located at nonequivalent positions on the structural scaffold (*63*). Therefore, it is not unreasonable to expect that the histidine residues in BFD play roles similar to the roles of those in PDC. The X-ray structures indicate that H70 will have a counterpart in H114 or H115 for *S. cerevisiae* PDC (*Y*PDC) or *Z. mobilis* PDC (*Zm*PDC), respectively. The counterparts for H281 are H113 and H114 for *Y*PDC and *Zm*PDC, respectively. For *Zm*PDC, it has been concluded that H113 is more critical for activity and is involved in the steps up to and including decarboxylation (*37*) while H114 may play a role in orienting one of the intermediates in the catalytic pathway (*37*). Variants at the corresponding sites in *Y*PDC exhibit similar reductions in specific activities. However, there were some significant, unexpected and unexplained differences in behavior with similar substitutions at the corresponding histidines in *Zm*PDC and *Y*PDC (*40*). BFD, too, differed from PDC with H70 (*Y*PDC H115) playing a more significant role than H281 (*Y*PDC H114), and certainly playing a role beyond the decarboxylation step.

Clearly, the assignment of the roles of active site residues is neither trivial nor intuitive. This is further exemplified by reexamination of our initial suggestion that S26 in BFD may play the same role as D28 in *Y*PDC (D27 in *Zm*PDC). The binding data clearly implicate S26 in the binding of the benzoylformate. Conversely, D27E and D27N variants of *Zm*PDC (*38*) and the D28A variant of *Y*PDC (*40*) show little change in the value of K_m, and it has been concluded that the aspartate residue is more important in the deprotonation of 2-α-hydroxyethyl-ThDP and concomitant product release than in substrate binding (*40*, *41*). In contrast, in BFD, H70 seems to be the base that deprotonates the analogous 2-α-hydroxybenzyl-ThDP. Therefore, although intuition may suggest otherwise, it appears that the two decarboxylases have evolved so that different amino acid types can fulfill the same role. Most remarkably, D28 in *Y*PDC and S26 in BFD both appear to have a role in aligning the initial ThDP adduct for decarboxylation, whereas D28 (*Y*PDC) and H70 (BFD) participate in product release.

ACKNOWLEDGMENT

Facilities shared by the Structural Biology group at Purdue University have been developed and supported by grants from the NIH, the NSF, the Lucille P. Markey Foundation, the Keck Foundation, and the office of the university executive vice president for academic affairs. Susan Brophy and Dr. Tanya Lodics have given us scientific help. Prof. William Cramer has provided the use of his spectrometer; Dr. Magdalen Lindenberg has assisted with stopped-flow data collection, and Dr. Stanislav Zakharov helped in the collection of the CD spectra.

REFERENCES

1. Halpin, R. A., Hegeman, G. D., and Kenyon, G. L. (1981) *Biochemistry 20*, 1525−1533.
2. Hegeman, G. D. (1966) *J. Bacteriol. 91*, 1140−1154.
3. Hegeman, G. D. (1966) *J. Bacteriol. 91*, 1155−1160.
4. Hegeman, G. D. (1966) *J. Bacteriol. 91*, 1161−1167.
5. Hegeman, G. D. (1970) *Methods Enzymol. 17A*, 674−678.
6. Rosenberg, S. L., and Hegeman, G. D. (1971) *J. Bacteriol. 108*, 1270−1276.
7. Durham, D. R. (1984) *J. Bacteriol. 160*, 778−780.
8. Petsko, G. A., Kenyon, G. L., Gerlt, J. A., Ringe, D., and Kozarich, J. W. (1993) *Trends Biochem. Sci. 18*, 372−376.
9. Hasson, M. S., Muskate, A., McLeish, M. J., Polovnikova, L. S., Gerlt, J. A., Kenyon, G. L., Petsko, G. A., and Ringe, D. (1998) *Biochemistry 37*, 9918−9930.
10. Hasson, M. S., Muscate, A., Henehan, G. T., Guidinger, P. F., Petsko, G. A., Ringe, D., and Kenyon, G. L. (1995) *Protein Sci. 4*, 955−959.
11. Sergienko, E. A., Wang, J., Polovnikova, L., Hasson, M. S., McLeish, M., Kenyon, G. L., and Jordan, F. (2000) *Biochemistry 39*, 13862−13869.
12. Kluger, R. (1997) *Pure Appl. Chem. 69*, 1957−1967.
13. Weiss, P. M., Garcia, G. A., Kenyon, G. L., Cleland, W. W., and Cook, P. F. (1988) *Biochemistry 27*, 2197−2205.
14. Reynolds, L. J., Garcia, G. A., Kozarich, J. W., and Kenyon, G. L. (1988) *Biochemistry 27*, 5530−5538.
15. Kern, D., Kern, G., Neef, H., Tittmann, K., Killenberg-Jabs, M., Wikner, C., Schneider, G., and Hubner, G. (1997) *Science 275*, 67−70.
16. Hubner, G., Tittmann, K., Killenberg-Jabs, M., Schaffner, J., Spinka, M., Neef, H., Kern, D., Kern, G., Schneider, G., Wikner, C., and Ghisla, S. (1998) *Biochim. Biophys. Acta 1385*, 221−228.
17. Jordan, F., Kudzin, Z. H., and Rios, C. B. (1987) *J. Am. Chem. Soc. 109*, 4415−4416.
18. Jordan, F., Li, H., and Brown, A. (1999) *Biochemistry 38*, 6369−6373.
19. Menon-Rudolph, S., Nishikawa, S., Zeng, X. P., and Jordan, F. (1992) *J. Am. Chem. Soc. 114*, 10110−10112.
20. Zeng, X., Chung, A., Haran, M., and Jordan, F. (1991) *J. Am. Chem. Soc. 113*, 5842−5849.
21. Arjunan, P., Umland, T., Dyda, F., Swaminathan, S., Furey, W., Sax, M., Farrenkopf, B., Gao, Y., Zhang, D., and Jordan, F. (1996) *J. Mol. Biol. 256*, 590−600.
22. Dobritzsch, D., Konig, S., Schneider, G., and Lu, G. (1998) *J. Biol. Chem. 273*, 20196−20204.
23. Furey, W., Arjunan, P., Chen, L., Sax, M., Guo, F., and Jordan, F. (1998) *Biochim. Biophys. Acta 1385*, 253−270.
24. Konig, S., Schellenberger, A., Neef, H., and Schneider, G. (1994) *J. Biol. Chem. 269*, 10879−10882.
25. Lindqvist, Y., Schneider, G., Ermler, U., and Sundstrom, M. (1992) *EMBO J. 11*, 2373−2379.
26. Mattevi, A., Obmolova, G., Schulze, E., Kalk, K. H., Westphal, A. H., de Kok, A., and Hol, W. G. (1992) *Science 255*, 1544−1550.
27. Muller, Y. A., Lindqvist, Y., Furey, W., Schulz, G. E., Jordan, F., and Schneider, G. (1993) *Structure 1*, 95−103.
28. Muller, Y. A., Schumacher, G., Rudolph, R., and Schulz, G. E. (1994) *J. Mol. Biol. 237*, 315−335.
29. Nikkola, M., Lindqvist, Y., and Schneider, G. (1994) *J. Mol. Biol. 238*, 387−404.
30. Nilsson, U., Lindqvist, Y., Kluger, R., and Schneider, G. (1993) *FEBS Lett. 326*, 145−148.
31. Robinson, B. H., and Chun, K. (1993) *FEBS Lett. 328*, 99−102.
32. Chabriere, E., Vernede, X., Guigliarelli, B., Charon, M. H., Hatchikian, E. C., and Fontecilla-Camps, J. C. (2001) *Science 294*, 2559−2563.
33. Charon, M. H., Volbeda, A., Chabriere, E., Pieulle, L., and Fontecilla-Camps, J. C. (1999) *Curr. Opin. Struct. Biol. 9*, 663−669.
34. Arjunan, P., Nemeria, N., Brunskill, A., Chandrasekhar, K., Sax, M., Yan, Y., Jordan, F., Guest, J. R., and Furey, W. (2002) *Biochemistry 41*, 5213−5221.

35. Moore, I. F., and Kluger, R. (2002) *J. Am. Chem. Soc. 124*, 1669−1673.
36. Schenk, G., Leeper, F. J., England, R., Nixon, P. F., and Duggleby, R. G. (1997) *Eur. J. Biochem. 248*, 63−71.
37. Candy, J. M., and Duggleby, R. G. (1998) *Biochim. Biophys. Acta 1385*, 323−338.
38. Chang, A. K., Nixon, P. F., and Duggleby, R. G. (1999) *Biochem. J. 339*, 255−260.
39. Guo, F., Zhang, D., Kahyaoglu, A., Farid, R. S., and Jordan, F. (1998) *Biochemistry 37*, 13379−13391.
40. Liu, M., Sergienko, E. A., Guo, F., Wang, J., Tittmann, K., Hubner, G., Furey, W., and Jordan, F. (2001) *Biochemistry 40*, 7355−7368.
41. Sergienko, E. A., and Jordan, F. (2001) *Biochemistry 40*, 7369−7381.
42. Lu, G., Dobritzsch, D., Baumann, S., Schneider, G., and Konig, S. (2000) *Eur. J. Biochem. 267*, 861−868.
43. Tsou, A. Y., Ransom, S. C., Gerlt, J. A., Buechter, D. D., Babbitt, P. C., and Kenyon, G. L. (1990) *Biochemistry 29*, 9856−9862.
44. Bradford, M. M. (1976) *Anal. Biochem. 86*, 142−146.
45. Ducruix, A., and Giegé, R. (1992) *Crystallization of nucleic acids and proteins: a practical approach*, IRL Press at Oxford University Press, Oxford, England.
46. Gewirth, D. (1996) *The HKL Manual*, 5th ed., Purdue University, West Lafayette, IN.
47. Otwinowski, Z., and Minor, W. (1996) *Methods Enzymol. 276*, 307−325.
48. Navaza, J. (1994) *Acta Crystallogr. A50*, 157−163.
49. Bailey, S. (1994) *Acta Crystallogr. D50*, 760−763.
50. Jones, T. A., Zou, J. Y., Cowan, S. W., and Kjeldgaard, M. (1991) *Acta Crystallogr. A47*, 110−119.
51. Brunger, A. T. (1992) *XPLOR: A system for X-ray crystallography and NMR*, Yale University Press, New Haven, CT.
52. Brunger, A. T., Adams, P. D., Clore, G. M., Delano, W. L., Gros, P., Grosse-Kunstleve, R. W., Jiang, J.-S., Kuszewski, J., Nilges, M., Pannu, N. S., Read, R. J., Rice, L. M., Simonson, T., and Warren, G. L. (1998) *Acta Crystallogr. D54*, 905−921.
53. Kleywegt, G. J., and Jones, T. A. (1998) *Acta Crystallogr. D54*, 1119−1131.
54. Carson, M. (1997) in *Macromolecular Crystallography* (Carter, C. W., Jr., and Sweet, R. M., Eds.) pp 493−504, Academic Press, New York.
55. Cornish-Bowden, A. (1995) *Fundamentals of enzyme kinetics*, Portland, London.
56. Li, H., and Jordan, F. (1999) *Biochemistry 38*, 10004−10012.
57. Li, H., Furey, W., and Jordan, F. (1999) *Biochemistry 38*, 9992−10003.
58. Woody, R. W., and Dunker, A. K. (1996) in *Circular Dichroism and the Conformational Analysis of Biomolecules* (Fasman, G. D., Ed.) pp 109−157, Plenum Press, New York.
59. Bernasconi, C. F. (1976) *Relaxation Kinetics*, Academic Press, New York.
60. Lu, G., Dobritzsch, D., Konig, S., and Schneider, G. (1997) *FEBS Lett. 403*, 249−253.
61. Sergienko, E. A., and Jordan, F. (2001) *Biochemistry 40*, 7382−7403.
62. Dyda, F., Furey, W., Swaminathan, S., Sax, M., Farrenkopf, B., and Jordan, F. (1993) *Biochemistry 32*, 6165−6170.
63. Todd, A. E., Orengo, C. A., and Thornton, J. M. (2002) *Trends Biochem. Sci. 27*, 419−426.

BI026490K